

Single-shot energy measurement of a single atom and the direct reconstruction of its energy distribution

Ziv Meir, Tomas Sikorsky, Nitzan Akerman, Ruti Ben-shlomi, Meirav Pinkas, and Roei Ozeri

Department of Physics of Complex Systems, Weizmann Institute of Science, Rehovot 7610001, Israel

(Received 11 June 2017; published 23 August 2017)

An ensemble of atoms in a steady state, whether or not in thermal equilibrium, has a well-defined energy distribution. Since the energy of single atoms within the ensemble cannot be individually measured, energy distributions are typically inferred from statistical averages. Here, we show how to measure the energy of a single atom in a single experimental realization (single shot). The energy distribution of the atom over many experimental realizations can thus be readily and directly obtained. We apply this method to a single ion trapped in a linear Paul trap for which the energy measurement in a single shot is applicable from $10 \text{ K} \times k_B$ and above. Our energy measurement agrees within 5% to a different thermometry method which requires extensive averaging. Apart from the total energy, we also show that the motion of the ion in different trap modes can be distinguished. We believe that this method will have profound implications on single-particle chemistry and collision experiments.

DOI: [10.1103/PhysRevA.96.020701](https://doi.org/10.1103/PhysRevA.96.020701)

Thermometry is a fundamental tool in the natural sciences [1]. A single-atom system can be classically assigned with a well-defined energy at any given moment in time. Temperature or, more generally, energy distribution arises when the energy is recorded over many identical experimental realizations [2]. Typically, a reliable measurement of a single atom's energy in a single experimental realization is not possible. Hence, the energy distribution is inferred from the average over multiple experimental realizations and with an assumption on the underlying distribution function [3–5].

Here, we propose and implement a method to directly measure the energy of a single trapped atom in a single experimental realization. We detect the atom's fluorescence during the process of laser Doppler cooling from which we extract the atom's energy in a “single shot”. The atom's energy distribution over multiple realizations is thus directly measured without any prior assumptions.

Our method is based on Doppler cooling thermometry [3,5], which is a well-known technique for trapped atoms in the energy regime starting from the mK range up to a few K. Here, we extend this method to a regime of higher energies in which the high nonlinearity of the fluorescence signal in time allows for the exact determination of the atom's energy in a single measurement. The extension of Doppler thermometry to 100's and even 1000's K opens experimental avenues for the determination and analysis of exothermic processes [6–17] and out-of-equilibrium dynamics [18,19].

Our model calculates the trapped particle motion and density matrix of internal states during the process of Doppler cooling by solving the classical equations of motion (EOM) [Eqs. (1) and (2)] and the time-dependent optical Bloch equations (OBEs) [Eq. (3)] simultaneously. These sets of equations are coupled through motion induced Doppler shifts of internal transitions and lasers beams' finite size induced Rabi frequency modulation. This method is applicable for any particle with closed-cycling cooling transitions [20–22].

Here, we consider a single $^{88}\text{Sr}^+$ ion trapped in a linear rf Paul trap (see Ref. [23] for details regarding the experimental apparatus) subject to close-to-resonance cooling (422 nm) and repump (1092 nm) laser beams. The eight energy levels

participating in the cooling process are shown in Fig. 1(a). The experimental orientation of the ion Paul trap and the lasers is given in Figs. 1(b) and 1(c).

The ion's EOM are given by

$$\dot{x}_i = v_i, \quad (1)$$

$$\begin{aligned} \dot{v}_i = & -x_i(a_i + 2q_i \cos(\Omega_{\text{rf}}t))\Omega_{\text{rf}}^2/4 \\ & + \hbar \rho_e (\Gamma_{422} k_{i,422} + \Gamma_{1092} k_{i,1092})/m. \end{aligned} \quad (2)$$

Here, a_i and q_i are the Mathieu trap parameters which determine the trap's static and rf (frequency $\Omega_{\text{rf}}/2\pi$) quadrupole electric fields magnitudes, respectively [24]. The second term in Eq. (2) is the effective cooling force generated by the absorption and spontaneous emission of the lasers photons [20]. We neglect the dipole force in our calculation since we use free-running beams and a relatively large focus. This force should be included when implementing, e.g., a standing-wave or optical-tweezer beam configuration. The transitions linewidths are $\Gamma_{422}/2\pi = 20.37 \text{ MHz}$ and $\Gamma_{1092}/2\pi = 1.18 \text{ MHz}$, and k_i are the laser k -vector projections on the different trap modes ($i = x, y, z$). Planck's constant is \hbar and m is the ion's mass. The excited-state population is given by $\rho_e = \rho_{33} + \rho_{44}$, where $\rho_{ij} = \langle \psi_i | \hat{\rho} | \psi_j \rangle$, $|\psi_{3|4}\rangle = |P_{1/2}, m = \mp 1/2\rangle$, and $\hat{\rho}$ is the ion's density matrix. We write the time evolution of $\hat{\rho}$ in the form of a Lindblad master equation,

$$\frac{d\hat{\rho}}{dt} = -\frac{i}{\hbar} [\hat{H}, \hat{\rho}] + \hat{D}. \quad (3)$$

Here, \hat{H} is the system Hamiltonian which is composed of the atomic energy levels and the light-matter interaction terms. \hat{D} is the Lindblad operator which includes dissipative terms such as spontaneous decay (see Refs. [5,25] for further details).

Our numerical results are shown in Fig. 2 (light green lines). The ion's initial amplitude corresponds to 225 K in the axial mode while the amplitudes in the other modes are set to zero. We plot the ion's secular energy (dashed green line in Fig. 2) defined as $E_{\text{ion}}(t) = \sum_i m \omega_i^2 x_{0,i}(t)^2/2$, where ω_i are the trap secular frequencies and $x_{0,i}$ are the secular amplitudes calculated using the first-order solution of the

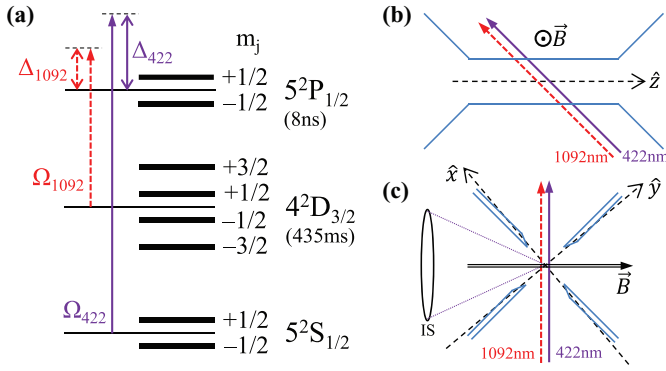


FIG. 1. (a) $^{88}\text{Sr}^+$ energy levels. The three energy manifolds which participate in Doppler cooling are the $5^2S_{1/2}$ ground state, the $4^2D_{3/2}$ metastable state, and the $5^2P_{1/2}$ excited state. Each manifold splits under magnetic field according to the projection of total angular momentum on the magnetic field axis m_j . The lifetimes of energy levels are given in brackets. Cooling beam (solid purple arrow) and repump beam (dashed red arrow) are indicated together with their corresponding detuning ($\Delta_{422}/2\pi = -19$ MHz, $\Delta_{1092}/2\pi = 0$ MHz, double-sided arrow) and Rabi frequencies ($\Omega_{422}/\Gamma_{422} = 0.5$ and $\Omega_{1092}/\Gamma_{1092} = 8$). The diagram is not to scale. (b) Side view of experimental setup. Cooling (solid purple arrow) and repump (dashed red arrow) beams are copropagating, 46° with respect to the axial (\hat{z}) axis of the ion trap (trap electrodes in light blue lines). (c) Front view of experimental setup. The beam projection on the ion trap's radial plane is 40° with respect to the radial \hat{x} mode. The magnetic field, $|\vec{B}| = 3 \pm 0.02$ G, quantization axis is perpendicular to the cooling and repump beams. The beams' linear polarization angles (not shown) are 6° and 35° with respect to the magnetic field for the cooling and repump, respectively. The imaging system (IS) collects only 422 nm photons. The collection efficiency (the ratio of photons collected to photons scattered) is $1/(190 \pm 2)$.

Mathieu equations [Eq. (2) without the damping term] [24]. We also plot the fluorescence rate defined as $\Gamma_{\text{ion}}(t) = \Gamma_{422}\rho_e(t)$ (solid green line).

The fluorescence signal features high nonlinearity in time. As the ion cools down, fluorescence is maintained at a low rate of ~ 350 kHz and almost does not increase for ~ 350 ms until the ion reaches an energy of ~ 25 K. At this point, the fluorescence rate increases rapidly, within a few ms, to the steady-state value of ~ 8.7 MHz. Previous Doppler cooling thermometry [3,5] was performed in the latter regime, where the fluorescence signal changes significantly and rapidly during the cooling process. Due to the short time scale, typically a few ms, of the dynamics in this regime, the signal-to-noise ratio is poor and averaging over many experimental realizations is required. In the single-shot Doppler thermometry presented here, we focus on the former regime. We exploit the high nonlinearity characterized by the sharp rise in the fluorescence rate at the end of the cooling dynamics to precisely determine the time it takes the ion to cool down. Furthermore, because we rely on identifying a single time point rather than measuring an average number of photons, our method is therefore almost insensitive to photon shot noise and thus does not require averaging. Using our simulation we can translate the initial energy to cooling time and vice versa (see Fig. 2).

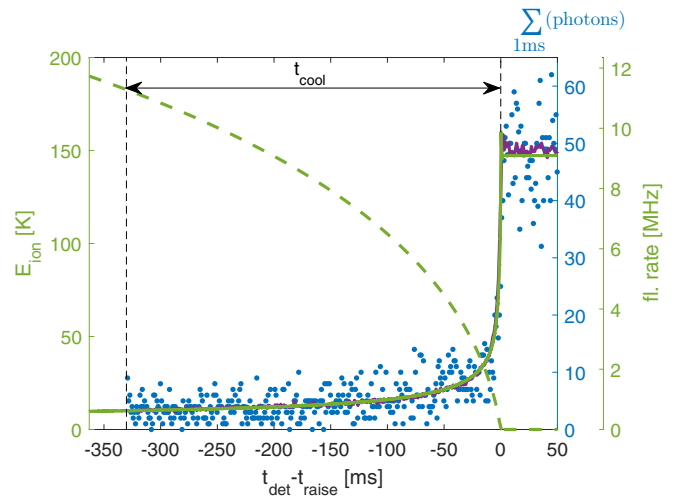


FIG. 2. Axial mode single-shot energy measurement. Ion's secular energy (dashed light green line) and fluorescence rate (solid light green line) derived from the numerical solution of Eqs. (1)–(3) where the initial energy is only in the axial mode. Blue points are a single experimental realization measured fluorescence rate using 1-ms time binning. We find the cooling time, $t_{\text{cool}} = 330.2 \pm 0.6$ ms, using maximum likelihood analysis. From the cooling time, we extract the ion's initial energy, $E_{\text{ion}} = 182.74 \pm 0.14$ K. Errors account only for statistical noise (fit confidence). The dark purple line is the average over 100 identical experimental realizations.

We compare the numerical results of the fluorescence rate to the one observed in experiment. We trap a single $^{88}\text{Sr}^+$ ion and cool it to the Doppler temperature (0.5 mK). We then increase its kinetic energy significantly in the axial mode using an oscillating electric field pulse close to resonance ($\delta = 2\pi \times 150$ Hz) with the axial mode frequency ($\omega_z = 418.561(3)$ kHz). We detect the ion's fluorescence using a photon counter in 1-ms time bins. For our experimental parameters, this amounts to ~ 3 photons/bin at the beginning and ~ 50 photons/bin at the end of the fluorescence signal. A single-shot experimental result is shown in Fig. 2 (blue dots). We use a maximum likelihood analysis to match the experimental cooling time data to the numerical results using a single fit parameter, the ion's initial energy. We estimate an initial energy of $E_{\text{ion}} \approx 183$ K. Our numerical results agree very well with the single-shot experimental data (blue dots) and also with an average over 100 experimental realizations (solid dark purple line). The statistical noise in determining the cooling time introduces only a small error (see the Fig. 2 caption) compared to the error due to the uncertainty in the numerical calculation parameters. We estimate the latter error to be on the level of $\sim 2\%$ for this energy regime [26].

To test the accuracy of our energy measurement, we compare our high-energy results to a different low-energy measurement scheme by comparing the fitted experimental parameters of both methods. In both experiments, we heat the ion using a close-to-resonance oscillating electric field pulse on the trap electrodes. We model the heating using a nondamped driven harmonic oscillator EOM together with a cubic nonlinear term [27],

$$\ddot{z} + \omega_z^2 z + (\omega_z/z_{\text{nl}})^2 z^3 = eE_d \cos[(\omega_z + \delta)t]/m. \quad (4)$$

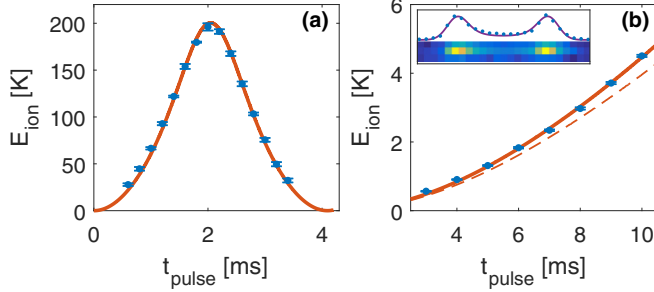


FIG. 3. Comparison of two thermometry methods. (a) Dots are energies extracted using the single-shot Doppler cooling thermometry. Each data point is the average of six experiments. Error bars are the standard deviation of repeated experiments. The line is a fit to the solution of Eq. (4) with two fit parameters, z_{nl} and $E_{d,1}$. (b) Dots are energies extracted from measuring the ion's amplitude on a CCD (inset). The solid line is a fit with two parameters, $E_{d,2}$ and δ . The dashed line is a numerical calculation using the electric fields $E_{d,2}$, calculated from $E_{d,1}$, which graphically shows the small systematic error between the methods.

Here, z_{nl} accounts for the trap nonlinearity, E_d is the electric field drive amplitude, and δ is the drive frequency detuning from the axial resonance ω_z . We can treat only a single axis of the ion trap since the detuning of the drive from the other modes is large (100's kHz). We use the harmonic oscillator equation instead of the Mathieu equation [Eq. (2)] since the rf fields' amplitude along the axial direction in our trap is negligible and trapping in this direction is solely due to static fields [23].

In the first experiment, we scan the drive pulse time and measure the ion energy using our single-shot energy measurement. We observe a periodic oscillation of the ion energy as expected from a driven, nondamped harmonic oscillator [28]. However, the period of this oscillation (~ 4 ms) is faster than what we expect from the detuning of our driving field ($1/150$ Hz = 6.67 ms). The fast oscillations occur due to the trap nonlinearity, which becomes important in this energy regime. As the ion oscillation amplitude increases, nonlinearity pulls the trap frequency away such that the effective detuning increases.

We numerically solve Eq. (4) with the initial conditions of an ion at rest in the center of the trap. We calculate the total ion energy, $E_{ion}(t) = m(\omega_z^2 z^2(t) + \dot{z}^2(t))/2$, as a function of the pulse time. We fit the solution to the experimental results with two fit parameters, the trap nonlinearity ($z_{nl} = 1146 \pm 5 \mu\text{m}$) and the electric field amplitude ($E_{d,1} = 197.7 \pm 1.3$ mV/m). The fit and experimental results are shown in Fig. 3(a). The electric field value is necessary for the comparison of our thermometry with an independent method, as shown below. The nonlinearity coefficient is a measure of the Paul trap anharmonicity. To measure this trap parameter, high-energy motional excitation of the ion is required, as in the method presented here. Characterization of the anharmonicity in Paul traps is important, e.g., in the field of mass spectrometry [29].

In the second, low-energy experiment, we also scan the drive pulse time, however, with a much lower drive amplitude. We measure the ion oscillation amplitude by imaging the

fluorescence spatial distribution on a CCD, from which we can derive the ion's energy [Fig. 3(b) inset]. The data were taken from Ref. [5]. Due to the mechanical effects of fluorescence on the ion, we scatter only a few photons in each experimental repetition and repeat 5000 times to improve our signal-to-noise ratio. Due to the ion's oscillatory motion, the fluorescence stretches along the axis of motion. We extract the oscillation amplitude from a fit to a model which takes into account the effect of Doppler shifts on the fluorescence [purple line in the Fig. 3(b) inset [26]]. We fit Eq. (4) solution to the experimental results with two fit parameters, the electric field amplitude ($E_{d,2} = 5.89 \pm 0.09$ mV/m) and the drive detuning ($\delta = 2\pi \times 30 \pm 2$ Hz) which was not recorded in this experiment. The nonlinear parameter z_{nl} is taken from the first experiment results and is negligible at this energy regime. The fit and data are shown in Fig. 3(b).

We decreased the electric field amplitude in the second experiment by a factor of 35.5 by decreasing the drive power by 31 dB. This expected ratio between the electric fields agrees well with the experimentally measured ratio of $E_{d,1}/E_{d,2} = 33.6 \pm 0.6$. The two methods thus agree to within 5%.

Thus far we treated only the case of a single mode participating in the cooling process. However, there are experimental situations in which the particle's initial energy is distributed among the three modes of the trap and, moreover, this distribution is *a priori* unknown. The cooling dynamics of the three trap modes is different: first, due to the different projections of the cooling lasers along the modes axes, and second, due to the spectrum dependence on the modes' energy distribution through micromotion [5].

In linear Paul traps, the axial confinement is harmonic, hence the motion contains a single spectral component, usually at a relatively low frequency of up to a few MHz. The radial motion, however, contains also fast oscillation in the 10's MHz range, which is known as inherent micromotion. At large oscillation amplitudes, the spectrum significantly changes due to the appearance of sidebands [5,30]. These sidebands broaden the spectrum, leading to increased fluorescence. As the ion cools, the broad spectrum leads to slower cooling of the radial modes with respect to the cooling rate of the axial mode. The energy dynamics as well as the fluorescence dynamics when the ion is initialized in one of the three different modes (x red, y light blue, and z green) are shown in Fig. 4. Here, the trap frequencies in the three modes were $\omega/2\pi = (720, 980, 418)$ kHz and the trap rf frequency was $\Omega_{rf}/2\pi = 26.51$ MHz.

A comparison with experimental data in the radial mode is also given in Fig. 4 (blue dots). The experimental setup is the same as in Fig. 2, only now we used a pulse close to resonance with the x -radial mode, and a pulse time of $\sim 50 \mu\text{s}$. We see that the experimental fluorescence agrees well with the numerically calculated curve results for an ion prepared in one of the radial modes. While the radial x - and y -mode curves are very similar, the axial mode curve is well distinguished such that a single-shot experiment is clearly sufficient to determine whether the energy was initiated in the radial or the axial modes. Below, we will show that the radial modes are also distinguishable in a single shot, however, with reduced confidence. Interpreting the cooling signal in the wrong mode can lead to an error in the energy estimation, as can be seen in Fig. 4.

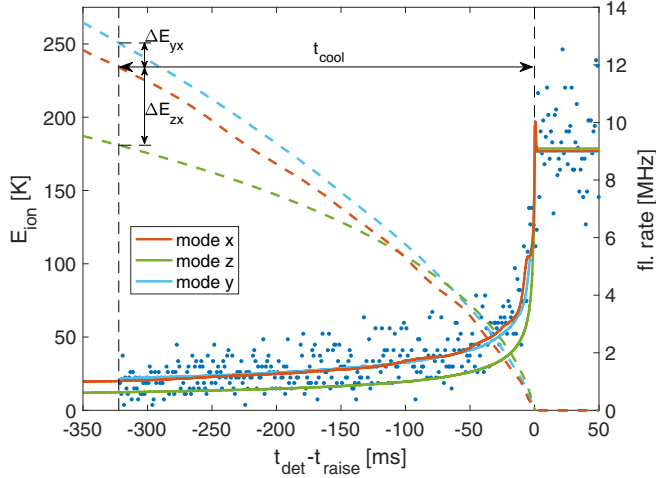


FIG. 4. Radial mode single-shot energy measurement. Ion's secular energy (dashed lines) and fluorescence rate (solid lines) derived from the numerical solution of Eqs. (1)–(3) where the initial energy is in the x -radial mode (red), y -radial mode (light blue), and z -axial mode (green, same as in Fig. 2). The dashed red and light blue lines are averaged over an rf cycle. Blue points are an example of a single experimental realization measured fluorescence of an ion prepared in the x -radial mode. The cooling time $t_{\text{cool}} = 322.2 \pm 1.3$ ms translates to $E_{\text{ion}} = 234.3 \pm 0.6$ K using the x -radial mode numerically calculated curve. Errors are due to statistical noise which affects the fitting. If we interpret the data using the z -axial curve, we underestimate the ion's energy by $\Delta E_{zx} \approx -53$ K. If we use the y -radial mode curve, we overestimate the ion's energy by $\Delta E_{yx} \approx 16$ K.

To test the confidence with which we can determine the mode in which the ion was excited, we perform the following experiment: We heat the ion using a close-to-resonance pulse, 100 times in each of the three different modes of the trap. We calculate, for each single-shot fluorescence data \mathbf{x} , the likelihood \mathcal{L} that it corresponds to either one of the three numerically calculated curves of an ion initialized in one of the three different modes shown in Fig. 4. Using the Poisson statistics of photon detection, we can write

$$\mathcal{L}_i(\mathbf{x}|\theta_i) = \prod_t \frac{\theta_{i|t}^{x_t} e^{-\theta_{i|t}}}{x_t!}. \quad (5)$$

Here, $\theta_{i|t}$ is one of the three curves ($i = x, y, z$) evaluated at the experimental cooling time t at which x_t photons were measured. The mode i in which the ion was initialized is determined according to a likelihood ratio test,

$$\frac{\mathcal{L}_i(\mathbf{x}|\theta_i)}{\mathcal{L}_j(\mathbf{x}|\theta_j)} > \eta = 1 \quad \forall j \neq i. \quad (6)$$

Here, we choose $\eta = 1$ such that type I errors (experiment in mode i is analyzed as $j \neq i$) and type II errors (experiment in mode $j \neq i$ is analyzed as i) are considered on equal footing. The results are shown in Fig. 5.

The likelihood ratio test succeeded in discriminating between the axial and the radial modes for all the experimental data. No axial experiments were detected as radial (type I error) nor were the radial experiments detected as axial

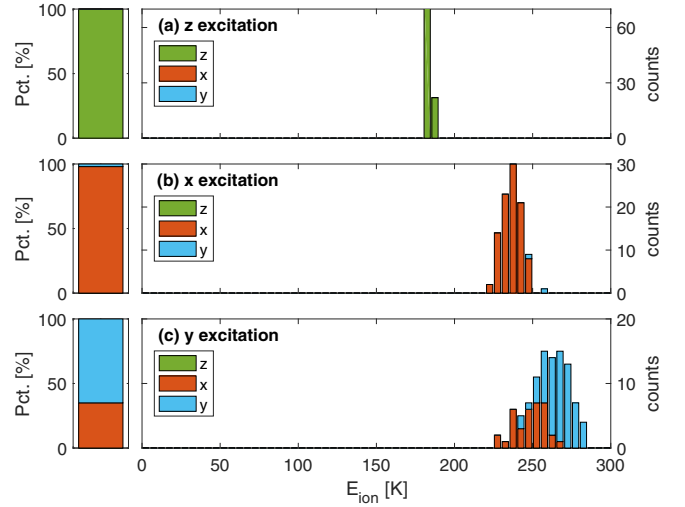


FIG. 5. Mode distinction and histogram reconstruction. Three different experiments in which the ion is heated only in the z -axial [top (a)], x -radial [middle (b)], and y -radial [bottom (c)] modes. We compare the experimental data to three numerically calculated curves (see Fig. 4) and choose the model with the maximal likelihood. The histograms on the right-hand side show the ion's energy derived using the maximum likelihood model. The left-hand bars show the initial energy mode distribution predicted by the model. Color indicates which model was used (z green, x red, y light blue).

(type II error). This result is not surprising since the axial and radials models are significantly different. We bound the type I and type II errors to less than 10^{-8} using a stochastic numerical simulation analysis.

Remarkably, when using the likelihood ratio test between the radial modes, we get 98% success and 65% success when the ion is prepared in the x and y modes, respectively. These are exceptional results considering the similarity of the radial numerical curves (Fig. 4, red and light blue solid lines). The expected successful discrimination between the x and y modes is $91 \pm 3\%$ for 100 repetitions, which is calculated using a stochastic numerical simulation. Here, the error reflects the statistical noise due to the limited number of experiments. The difference between the theoretical and experimental success rate in discriminating between the modes is due to a systematic error in our model which biases the results.

In Fig. 5 we also show how a single-shot measurement is used to reconstruct the ion's energy distribution in each of the modes. We plot a histogram of the ion's energies derived from our simulated model for each of the modes. In the axial mode experiment, we see a sharp Gaussian distribution. The distribution width (~ 2 K) is attributed to slightly different cooling laser parameters in each of the experimental realizations [26]. In the radial modes, the distribution is much wider (~ 6.5 K for the x mode and ~ 12.5 K for the y mode) due to the radial mode frequency variation [31] and an incorrect interpretation of the y -mode experiments as x mode.

To conclude, we show how to measure the energy of an atom in a single experimental realization and thus directly reconstruct its energy distribution. The reduced signal-to-noise ratio due to single-shot measurement does not influence the

accuracy of the method since it relies on a sharp nonlinear feature of the fluorescence time dynamics. The accuracy of the method relies on the accurate determination and control of the various experimental parameters which determine the cooling dynamics. In return, we can use it as a precision spectroscopy tool, e.g., to measure the trap anharmonicity. Using a likelihood analysis, we can determine the distribution of energy between the trap modes. This opens the door for different types of experiments, sensitive to events which redistribute the energy between the modes without significantly changing the total

energy, e.g., glancing collisions. This method is well suited for measuring the energy release in chemical reactions involving single atoms [8–11,13,15].

This work was supported by the Crown Photonics Center, ICore-Israeli excellence center circle of light, the Israeli Science Foundation, the U.S.-Israel Binational Science Foundation, and the European Research Council (Consolidator Grant No. 616919-Ionology). We thank Eran Ofek and Nir Davidson for their useful remarks.

-
- [1] M. R. Moldover, W. L. Tew, and H. W. Yoon, Advances in thermometry, *Nat. Phys.* **12**, 7 (2016).
- [2] D. Leibfried, R. Blatt, C. Monroe, and D. Wineland, Quantum dynamics of single trapped ions, *Rev. Mod. Phys.* **75**, 281 (2003).
- [3] J. H. Wesenberg *et al.*, Fluorescence during Doppler cooling of a single trapped atom, *Phys. Rev. A* **76**, 053416 (2007).
- [4] Z. Meir, T. Sikorsky, R. Ben-shlomi, N. Akerman, Y. Dallal, and R. Ozeri, Dynamics of a Ground-State Cooled Ion Colliding with Ultracold Atoms, *Phys. Rev. Lett.* **117**, 243401 (2016).
- [5] T. Sikorsky, Z. Meir, N. Akerman, R. Ben-shlomi, and R. Ozeri, Doppler cooling thermometry of a multilevel ion in the presence of micromotion, *Phys. Rev. A* **96**, 012519 (2017).
- [6] P. F. Staunum, K. Højbjerg, R. Wester, and M. Drewsen, Probing Isotope Effects in Chemical Reactions Using Single Ions, *Phys. Rev. Lett.* **100**, 243003 (2008).
- [7] S. Willitsch, M. T. Bell, A. D. Gingell, S. R. Procter, and T. P. Softley, Cold Reactive Collisions between Laser-Cooled Ions and Velocity-Selected Neutral Molecules, *Phys. Rev. Lett.* **100**, 043203 (2008).
- [8] F. H. J. Hall, M. Aymar, N. Bouloufa-Maafa, O. Dulieu, and S. Willitsch, Light-Assisted Ion-Neutral Reactive Processes in the Cold Regime: Radiative Molecule Formation Versus Charge Exchange, *Phys. Rev. Lett.* **107**, 243202 (2011).
- [9] W. G. Rellergert *et al.*, Measurement of a Large Chemical Reaction Rate Between Ultracold Closed-Shell ^{40}Ca Atoms and Open-Shell $^{174}\text{Yb}^+$ Ions Held in a Hybrid Atom-Ion Trap, *Phys. Rev. Lett.* **107**, 243201 (2011).
- [10] A. Härter, A. Krüchow, A. Brunner, W. Schnitzler, S. Schmid, and J. H. Denschlag, Single Ion as a Three-Body Reaction Center in an Ultracold Atomic Gas, *Phys. Rev. Lett.* **109**, 123201 (2012).
- [11] L. Ratschbacher, C. Zipkes, C. Sias, and M. Köhl, Controlling chemical reactions of a single particle, *Nat. Phys.* **8**, 649 (2012).
- [12] X. Tong *et al.*, State-selected ion-molecule reactions with Coulomb-crystallized molecular ions in traps, *Chem. Phys. Lett.* **547**, 1 (2012).
- [13] A. Krüchow, A. Mohammadi, A. Härter, J. H. Denschlag, J. Peres-Rios, and C. H. Greene, Energy Scaling of Cold Atom-Atom-Ion Three-Body Recombination, *Phys. Rev. Lett.* **116**, 193201 (2016).
- [14] A. Krüchow, A. Mohammadi, A. Härter, and J. Hecker Denschlag, Reactive two-body and three-body collisions of Ba^+ in an ultracold Rb gas, *Phys. Rev. A* **94**, 030701 (2016).
- [15] R. Saito, S. Haze, M. Sasakawa, R. Nakai, M. Raoult, H. Da Silva, Jr., O. Dulieu, and T. Mukaiyama, Characterization of charge-exchange collisions between ultracold ^6Li atoms and $^{40}\text{Yb}^+$ ions, *Phys. Rev. A* **95**, 032709 (2017).
- [16] T. Sikorsky, Z. Meir, R. Ben-shlomi, N. Akerman, and R. Ozeri, Spin controlled atom-ion inelastic collisions (unpublished).
- [17] R. Ben-shlomi *et al.*, Electronic-excitation exchange in ultracold ion-atom collisions (unpublished).
- [18] S. J. Schowalter *et al.*, Blue-sky bifurcation of ion energies and the limits of neutral-gas sympathetic cooling of trapped ions, *Nat. Commun.* **7** 12448 (2016).
- [19] Z. Meir, M. Pinkas, T. Sikorsky, R. Ben-shlomi, N. Akerman, and R. Ozeri, Direct observation of non-equilibrium dynamics in atom-ion collisions (unpublished).
- [20] D. J. Wineland and W. M. Itano, Laser cooling of atoms, *Phys. Rev. A* **20**, 1521 (1979).
- [21] E. S. Shuman, J. F. Barry, and D. DeMille, Laser cooling of a diatomic molecule, *Nature (London)* **467**, 820 (2010).
- [22] F. Lindenfelser, M. Marinelli, V. Negnevitsky, S. Ragg, and J. P. Home, Cooling atomic ions with visible and infra-red light, *New J. Phys.* **19**, 063041 (2017).
- [23] Z. Meir, T. Sikorsky, R. Ben-shlomi, N. Akerman, M. Pinkas, Y. Dallal, and R. Ozeri, Experimental apparatus for overlapping a ground-state cooled ion with ultracold atoms, [arXiv:1705.02686](https://arxiv.org/abs/1705.02686).
- [24] W. Paul, Electromagnetic traps for charged and neutral particles, *Rev. Mod. Phys.* **62**, 531 (1990).
- [25] H. Oberst, Resonance fluorescence of single barium ions, MSc thesis, Universität Hamburg, 1999.
- [26] See Supplemental Material at <http://link.aps.org/supplemental/10.1103/PhysRevA.96.020701> for details regarding experiment, numerical calculation, and CCD thermometry modeling.
- [27] N. Akerman, S. Kotler, Y. Glickman, Y. Dallal, A. Keselman, and R. Ozeri, Single-ion nonlinear mechanical oscillator, *Phys. Rev. A* **82**, 061402 (2010).
- [28] R. Ozeri, The trapped-ion qubit tool box, *Contemp. Phys.* **52**, 531 (2011).
- [29] A. A. Makarov, Resonance ejection from the Paul trap: A theoretical treatment incorporating a weak octapole field, *Anal. Chem.* **68**, 4257 (1996).
- [30] T. Pruttivarasin, M. Ramm, and H. Haefner, Direct spectroscopy of the $^2S_{1/2}-^2P_{1/2}$ and $^2D_{3/2}-^2P_{1/2}$ transitions and observation of micromotion modulated spectra in trapped Ca, *J. Phys. B* **47**, 135002 (2014).
- [31] K. G. Johnson *et al.*, Active stabilization of ion trap radiofrequency potentials, *Rev. Sci. Instrum.* **87**, 53110 (2016).